Optimization and Analysis of Wire-Wound Coil Heads for EMI Systems

Mark A. Reed, *Member, IEEE*, and Waymond R. Scott, Jr., *Fellow, IEEE*

***Abstract*— Many different coil head configurations are used in electromagnetic induction (EMI) systems for sensing buried targets; however, very little has been published on comparing the configurations. Comparing different coil head designs to one another is cumbersome because many factors determine how well different coil heads perform when constructed and attached to a system. Calculating the voltage received by a particular coil under ideal conditions is trivial, but this requires accounting for such factors as overall coil size, wire diameter, and conductivity. Comparing how only the winding geometries of various coil heads affect performance is much less straightforward. A set of normalized metrics that are independent of design decisions other than winding geometry are needed. This paper details a set of metrics for the characterization and comparison of EMI coil heads. These metrics are then used to optimize double-D, concentric, and dipole/quadrupole coil heads, which are then analyzed and compared to one another.**

***Index Terms*— Coil, electromagnetic, EMI, induction, optimization.**

I. Introduction

ELECTROMAGNETIC induction (EMI) systems used for subsurface sensing produce quasi-magnetostatic fields that create eddy currents in metallic targets. The eddy currents then produce secondary magnetic fields that are sensed by the system as an induced voltage at the terminals of the receive coil. Many of these systems have two separate coils—a transmit coil and a receive coil—located within a single head, as illustrated in Fig. 1 [1].

While quite good at detecting metal, the coils also interact with mineralized soil, which can induce a voltage at the terminals of the receive coil [2], [3]. If the soil is heavily mineralized or the targets are small or weakly conductive, this voltage can be significant. It is therefore desirable to consider the effects of the soil upon the received signal in addition to the more obvious target sensitivity.

Some of our previous work has dealt with creating coil heads through various optimization procedures [4]–[6]. During this work, it became apparent that adequately comparing different coil head designs to one another is cumbersome because many factors determine how well different coil heads perform when constructed and attached to a system. For example, coil dimensions, wire diameters, transmit power, amplifier noise, and winding geometry all influence both target sensitivity and soil sensitivity.

We are interested in comparing coil heads based only upon their winding geometry, so creating normalized target and soil sensitivity metrics that remove these extraneous factors is desirable. It is also important that the metrics be directly comparable and extensible to the stream function coil heads so that the metrics may be used in our future work on optimized coil heads.

There are not any existing methods of comparing coil heads for EMI systems that have these properties, nor does there appear to be any literature that compares coil heads fairly while accounting for both target and soil sensitivity using normalized metrics. For example, there are papers that design and compare EMI coils based on their ability to produce uniform fields and based on the behavior of their fields at specific locations [7], [8]. There are also papers that optimize and compare coils for maximum power transfer or to create optimal air-core magnetometers [9], [10]. Finally, work exists that compares various MRI coils and also work that compares a few common EMI coil types with respect to their performance in soil but not including target sensitivity [3], [11], [12]. None of these provides the overarching normalized metrics we need for comparing our optimized coils or a complete optimization and analysis of the performance of some of the coil types most commonly used in EMI systems.

After the creation of normalized coil metrics, yet another problem arises—both the target and soil sensitivity are multi-dimensional. Target sensitivity varies as the target is moved relative to the coil head, and soil sensitivity generally varies with the height of the coil head above the soil and the tilt of the head with respect to the soil. The multi-dimensionality must be reduced to ease coil head comparisons.

In the following sections, normalized metrics, which have been partially explored in our previous papers, are developed [13], [14]. The metrics are then used to optimize and compare double-D, dipole/quadrupole, and concentric coil heads to one another.

II. Target Sensitivity

When a conductive target is placed within the field produced by the transmit coil, energy is coupled between the transmit

Manuscript received October 19, 2018; accepted November 14, 2018. Date of publication November 29, 2018; date of current version February 6, 2019. This work was supported in part by the U.S. Office of Naval Research as a Multi-Disciplinary University Research Initiative on Sound and Electromagnetic Interacting Waves under Grant N00014-10-1-0958, in part by the U.S. Army REDCOM CERDEC Night Vision and Electronic Sensors Directorate, Science and Technology Division, Countermine Branch, and in part by the U.S. Army Research Office under Grant W911NF-11-1-0153. The associate editor coordinating the review of this paper and approving it for publication was Dr. Cheng-Ta Chiang. *(Corresponding author: Mark A. Reed.)*

The authors are with the School of Electrical and Computer Engineering, Georgia Institute of Technology, Atlanta, GA 30332 USA (e-mail: mark.reed@gatech.edu).

Digital Object Identifier 10.1109/JSEN.2018.2884175

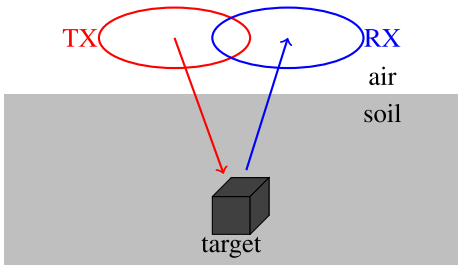

Fig. 1. Two-coil head illuminating a target buried in soil.

and receive coils through the target, resulting in an induced voltage at the terminals of the receive coil. This voltage can be—and often is—taken as a measure of target sensitivity.

Using reciprocity, the induced voltage can be written as

$$V_{\mathrm{r}} = j\omega\mu_0\, I_{\mathrm{TX}} \frac{\vec{H}_{\mathrm{RX}} \cdot \bar{\bar{m}} \cdot \vec{H}_{\mathrm{TX}}}{I_{\mathrm{RX}} I_{\mathrm{TX}}}, \tag{1}$$

where $\bar{\bar{m}}$ is the magnetic polarizability dyad of the target,[1] I_{TX} is the current flowing in the transmit coil, $\vec{H}_{\mathrm{TX}}$ is the transmit field at the target location, and $\vec{H}_{\mathrm{RX}}$ is the field that would be produced at the target location if the receive coil were driven by the current I_{RX} [15]. A comparison between coils using the expression in (1) is not as meaningful as it may appear. We cannot simply normalize by $j\omega\mu_0\, I_{\mathrm{TX}}$ and obtain a fair comparison between two different coil head designs.

A. Power Dissipation and Thermal Noise

The quantities $\vec{H}_{\mathrm{TX}}$ and $\vec{H}_{\mathrm{RX}}$ contain information about the geometries of the transmit and receive coils, respectively. However, the geometry can also include multiple turns of the same shape. For a given current, these turns effectively increase the field compared to a single turn, i.e. a dipole coil with multiple, identically shaped turns appears better than a dipole with a single turn if only V_{r} is considered. So, to fairly compare two coil heads, their sensitivities can be normalized by their lengths (effectively removing the advantage of extra turns).

The resistance of the coils is an important parameter that must be accounted for correctly because it directly impacts the power consumption of the transmit coil and the noise response of the receive coil. All else being equal, if one transmit coil dissipates less power than another, then the coil that heats less is superior. Similarly, receive coils that produce small amounts of thermal noise are desirable. Ideally, the dissipated power or thermal noise should be kept constant between coil heads that are being compared.

The resistance of a coil is easily computed if the current is assumed to be uniform in the wires:

$$R = \frac{l^2}{\sigma V}, \tag{2}$$

which in this form consists of the conductor length, l, the volume of the conductor, V, and the conductivity, σ.

[1]The target is assumed to be representable by the dipole model, and the fields across the target are assumed to be relatively uniform.

Increasing the conductivity or conductor volume and decreasing the length will decrease the dissipated power or thermal noise voltage of a coil, and vice versa.

These concepts can be introduced into the target sensitivity calculations. First, consider the power dissipated by the transmit coil,

$$P_{\mathrm{TX}} = \frac{l_{\mathrm{TX}}^2\, I_{\mathrm{TX}}^2}{\sigma V_{\mathrm{TX}}}. \tag{3}$$

Rearranging (3) results in an expression for the current,

$$I_{\mathrm{TX}} = \frac{\sqrt{P_{\mathrm{TX}} \sigma V_{\mathrm{TX}}}}{l_{\mathrm{TX}}}, \tag{4}$$

which can be substituted into the leftmost I_{TX} term in (1). I_{TX} can be assumed to be positive and real without loss of generality and is also assumed to be uniformly distributed in the wire.

Next, consider the expression for the the thermal noise voltage of the receive coil,

$$|V_{\mathrm{n}}| = \sqrt{4kT R_{\mathrm{RX}} \Delta f}, \tag{5}$$

where k is Boltzmann's constant, T is the temperature, R_{RX} is the resistance, and Δf is the bandwidth. Substituting the resistance of the receive coil, $R_{\mathrm{RX}} = l_{\mathrm{RX}}^2/\sigma V_{\mathrm{RX}}$ into the expression for the thermal noise voltage of the receive coil gives

$$|V_n| = \sqrt{\frac{4kT \Delta f l_{\mathrm{RX}}^2}{\sigma V_{\mathrm{RX}}}}. \tag{6}$$

It should be noted that only the thermal noise of the receive coil is considered in this paper. Other forms of noise such as environmental noise, amplifier noise, and motion induced noise are not considered.

B. Creating a Normalized Sensitivity

The transmit current expression from (4) can simply be substituted into the induced voltage equation, (1), but including the thermal noise voltage requires a ratio. This ratio is the SNR at the terminals at the receive coil, and it can be calculated by combining (1), (4), and (6) as

$$\frac{|V_{\mathrm{r}}|}{|V_{\mathrm{n}}|} = \frac{\omega\mu_0\sigma\sqrt{P_{\mathrm{TX}} V_{\mathrm{RX}} V_{\mathrm{TX}}}}{\sqrt{4\, kT \Delta f}} \frac{\vec{H}_{\mathrm{RX}} \cdot \bar{\bar{m}} \cdot \vec{H}_{\mathrm{TX}}}{I_{\mathrm{RX}} l_{\mathrm{RX}} I_{\mathrm{RX}} l_{\mathrm{RX}}}. \tag{7}$$

Note that the terms $\vec{H}_{\mathrm{TX}}/I_{\mathrm{TX}}$ and $\vec{H}_{\mathrm{RX}}/I_{\mathrm{RX}}$ are independent of the currents.

Quantities such as the transmit power, the volumes of the conductors, receiver bandwith, etc. influence the SNR, but they are not characteristics of winding patterns. It is therefore desirable to normalize the SNR by everything on the left half of (7). The remaining expression is multiplied by the fourth power of

the radius,[2] r—though other characteristic dimensions could be chosen—to make the normalized sensitivity independent of coil and system size (but not target size). We arrive at an expression for normalized target sensitivity,

$$\widehat{S}_{\mathrm{T}} = r^4 \frac{\vec{H}_{\mathrm{RX}} \cdot \hat{\bar{\bar{m}}} \cdot \vec{H}_{\mathrm{TX}}}{I_{\mathrm{RX}} l_{\mathrm{RX}} I_{\mathrm{TX}} l_{\mathrm{TX}}}, \tag{8}$$

where the magnetic polarizability of the target, $\bar{\bar{m}}$, has been normalized by its spectral norm: $\hat{\bar{\bar{m}}} = \bar{\bar{m}}/||\bar{\bar{m}}||$. Note that the sensitivity is a function of the symmetry of the target. For this work, $\bar{\bar{m}}$ is chosen to be the identity dyad, which represents an infinitesimal, spherical (rotationally symmetric) target.

III. Soil Sensitivity

Mineralized soil (soil where the magnitude of the magnetic susceptibility, χ, is nonzero) will induce a voltage in the receive coil by changing the effective coupling between the transmit and receive coils. This voltage[3] can be a significant problem if the soil is heavily mineralized or the target is small or weakly conductive. Comparing the performance of coils in mineralized soil is therefore important, so a normalized soil sensitivity metric will now be developed.

The voltage induced in the receive coil as a result of energy coupled through the soil between the transmit and receive coils can be written as

$$V_{\mathrm{s}} = j\omega\mu_0 \, I_{\mathrm{TX}} \int_{\mathrm{soil}} \chi \frac{\vec{H}_{\mathrm{TX}} \cdot \vec{H}_{\mathrm{RX}}}{I_{\mathrm{TX}} I_{\mathrm{RX}}} dV, \tag{9}$$

where χ is the magnetic susceptibility of the soil, and under the Born approximation, $\vec{H}_{\mathrm{TX}}$ and $\vec{H}_{\mathrm{RX}}$ are calculated in free space. This expression can be considerably simplified by recognizing that the method of images can be used and the Born approximation eschewed [16]. The integral can be written in terms of the mutual inductance, $\widehat{M}_{\widehat{\mathrm{TX}},\mathrm{RX}}$, between a transmit coil that is mirrored about the air/soil interface and the receive coil [3]:

$$V_{\mathrm{s}} = j\omega I_{\mathrm{TX}} \frac{\chi}{2+\chi} \widehat{M}_{\widehat{\mathrm{TX}},\mathrm{RX}}, \tag{10}$$

where the soil is assumed to be homogeneous and isotropic.

A cursory examination shows that (1) and (10) are similar. It is sensible to once again substitute (4) into (10) and divide by (6), which gives the following expression,

$$\frac{|V_{\mathrm{s}}|}{|V_{\mathrm{n}}|} = \frac{\omega\sigma\sqrt{P_{\mathrm{TX}} V_{\mathrm{RX}} V_{\mathrm{TX}}}}{\sqrt{4\,kT\Delta f}} \frac{\chi}{2+\chi} \frac{\widehat{M}_{\widehat{\mathrm{TX}},\mathrm{RX}}}{l_{\mathrm{TX}} l_{\mathrm{RX}}}. \tag{11}$$

[2]Care must be taken in choosing the characteristic dimension as it has a strong effect on the normalized sensitivity. For example, if square and round coils are being compared, choosing the radius of the round coils is clear, but for the square coils, choosing the radius to the center of the side or the corner makes a sqrt(2) difference in the radius. The sqrt(2) difference in the characteristic dimension results in a factor of 4 difference in the normalized sensitivity. The correct choice of the radius in this example depends on the physical constraints desired for the coils. One choice is correct if the coils are constrained to fit into a square and the other is correct if the coils are constrained to fit into a circle.

[3]Highly conductive soils can also induce an unwanted voltage in the receive coil. However, a treatment of the effects of conductive soils is beyond the scope of this paper.

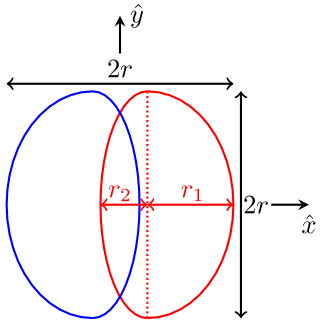

Fig. 2. Optimal double-D coil geometry enclosed in a bounding box showing semi-minor axes r_1 and r_2, with the transmit coil in red and the receive in blue.

Next, note that the mutual inductance can be written in terms of the coil fields as

$$\widehat{M}_{\widehat{\mathrm{TX}},\mathrm{RX}} = 2\mu_0 \int_{\mathrm{soil}} \frac{\vec{H}_{\mathrm{TX}} \cdot \vec{H}_{\mathrm{RX}}}{I_{\mathrm{TX}} I_{\mathrm{RX}}} dV, \tag{12}$$

so (11) must be normalized by the factor

$$2\mu_0 \frac{\omega\sigma\sqrt{P_{\mathrm{TX}} V_{\mathrm{RX}} V_{\mathrm{TX}}}}{\sqrt{4kT\Delta f}} \frac{\chi}{2+\chi} \tag{13}$$

to remove quantities that are not characteristics of the winding pattern and multiplied by the characteristic dimension, r, in order to make the normalized sensitivity independent of coil and system size. The result of these operations is the normalized soil sensitivity,

$$\widehat{S}_{\mathrm{s}} = r \frac{\widehat{M}_{\widehat{\mathrm{TX}},\mathrm{RX}}}{2\mu_0 \, l_{\mathrm{TX}} l_{\mathrm{RX}}}. \tag{14}$$

Note that the mutual inductance term can be calculated for arbitrary geometries easily using Neumann's formula [17], [18].

IV. Optimization Parameters

The target sensitivity, $\widehat{S}_{\mathrm{T}}$, of each coil head varies spatially in three dimensions, and the soil sensitivity, $\widehat{S}_{\mathrm{s}}$, varies with both the height of the coil head above the soil and its tilt relative to the soil. We will reduce the dimensionality of these parameters to help with comparisons, with the caveat that the choices are somewhat arbitrary, though we believe them to be apt for the coils being analyzed.

A. Mean Target Sensitivity

The coil heads that are being compared are all designed to be handheld, two-coil heads (with one transmit and one receive coil) that are intended primarily to be swept side-to-side by an operator. In general, it is desirable to have a sensitivity pattern[4] that is broad along the y-axis (down-track direction), while the pattern in the x-direction (cross-track) is less important (see Fig. 2) — in fact, a narrow cross-track pattern helps to

[4]Here we will consider the sensitivity "pattern" to be a quantity analogous to an antenna pattern that describes how well the coil head detects a target—in this case a sphere

improve target localization. Finally, good depth performance is obviously of interest.

We therefore have three dimensions to consider: x (cross-track), y (down-track), and z (depth). It is logical to calculate the sensitivity over a cube of some finite portion of the coil head's search region and then attempt to reduce the sensitivity pattern within this cube to a manageable quantity.

Knowledge of the general pattern shapes is useful in determining metrics for these coils. In particular, the double-D pattern is generally broad down-track and narrow cross-track with the peak close to the origin. The pattern of a concentric coil head is rotationally symmetric about the origin, and the pattern of a dipole/quadrupole peaks in the center of the two quadrupole loops while nulling on the y-axis.

Therefore, for some coils, such as the double-D and the dipole/quadrupole, it is first necessary to take the maximum of the sensitivity in the x-dimension of the sensitivity cube because the pattern is not centered:

$$\widehat{S}_{\mathrm{m}}(y,z) = \max_{x}\left(\left|\widehat{S}_{\mathrm{T}}(x,y,z)\right|\right). \tag{15}$$

This reduces the sensitivity cube to a 2-D sensitivity matrix that is a function of y and z.

Next, to encourage a broad downtrack pattern, the geometric mean over 80%[5] of the coil head's maximum dimension ($2r$) in the y-dimension is taken:

$$\widehat{S}_{\mathrm{gm}}(z) = \underset{y}{\mathrm{geo\_mean}}\left(\max_{x}\left(\left|\widehat{S}_{\mathrm{T}}(x,y,z)\right|\right)\right). \tag{16}$$

This results in a sensitivity metric that is a function only of z, reducing the 2-D sensitivity matrix to a sensitivity vector. A geometric mean rather than a max or an arithmetic mean is used because a broad pattern in the y-direction is desirable, and regions of poor sensitivity within the sensitivity cube are given more importance by a geometric mean than an arithmetic mean. For example, a single location with zero sensitivity will make the geometric mean zero.

$\widehat{S}_{\mathrm{gm}}$ is a function of depth, so another geometric mean is taken over $\widehat{S}_{\mathrm{gm}}$—this time in the z-dimension, reducing the sensitivity matrix to a scalar value—to create a volume target sensitivity metric.[6]

B. Soil Sensitivity

Like the target sensitivity, the soil sensitivity has multiple dimensions—it varies as the coil head is tilted relative to the soil (or as the surface of the ground becomes rough) and as the height of the head above the soil changes. However, we care most about the worst case within the normal range of soil heights and tilts over which the coils will be used. The soil response of all three coil head types generally increases as they are brought closer to the surface of the soil, but because coil heads are generally operated above a certain height and because the soil response will be calculated at each height with the coils tilted, we have arbitrarily chosen to calculate the soil response for the coil heads starting at $0.2r$ above the soil. In addition to the minimum height that has been chosen, it makes sense to calculate the soil sensitivity for various soil heights (h_{s}) and tilts (t_{c}) and then take the maximum over all heights ($0.2r < h_{\mathrm{s}} < 1.0r$) and tilts ($0 < t_{\mathrm{c}} < 10$ degrees) within a reasonable range. The rotational symmetry of the concentric head requires only one tilt angle while the double-D and dipole/quadrupole heads require two angles each.

Finally, low soil sensitivity is desirable but not at the expense of target sensitivity. To this end, it is desirable to balance good target sensitivity with low soil sensitivity, so it makes sense to take the ratio our various mean target sensitivity metrics and the maximum soil sensitivity:

$$\widehat{S}_{\mathrm{gms}} = \frac{\widehat{S}_{\mathrm{gm}}}{\max\left(\left|\widehat{S}_{\mathrm{s}}\right|\right)}, \tag{17}$$

and

$$\widehat{S}_{\mathrm{ggms}} = \frac{\widehat{S}_{\mathrm{ggm}}}{\max\left(\left|\widehat{S}_{\mathrm{s}}\right|\right)}. \tag{18}$$

C. Target Sensitivity Versus Soil Sensitivity

Designing coil heads with high target sensitivity and low soil sensitivity is desirable. However, these two traits are not always positively correlated, so both traits must be considered independently in an optimization. In the quest to design a good "all-around" coil head, trading off some raw target sensitivity for a large reduction in soil sensitivity is possibly desirable, but, obviously, reducing the target sensitivity too much in the quest for low soil sensitivity will negatively impact performance in lightly mineralized soils. A metric that strikes a balance between the two traits is necessary.

The metric $\widehat{S}_{\mathrm{ggm}}$ gives us a simple measure of target sensitivity. The metric $\widehat{S}_{\mathrm{ggms}}$ gives us a simple measure of the target sensitivity relative to the soil sensitivity, but it does not consider the absolute value of the target sensitivity. A coil with very poor target sensitivity can still appear very good if the soil sensitivity is negligible.

For this work, this is handled by making a parametric graph, Fig. 25, which plots $\widehat{S}_{\mathrm{ggm}}$ against $\widehat{S}_{\mathrm{ggms}}$ for a range of double-D coil parameters for all coil heads considered in this paper and is used to choose optimized double-D, concentric, and dipole/quadrupole coil heads. This considers both the target sensitivity of a coil head and the target sensitivity versus the soil sensitivity of a coil head. If lines of -1 slope (such as the dashed lines in Fig. 25) were drawn through each coil, the best performing coil head would be the one with the greatest y-intercept.

V. Coil Analysis

Now double-D, concentric, and dipole/quadrupole coil heads can be optimized. Each coil head type is characterized by one or two geometric parameters, which can be swept over reasonable ranges to vary the shape of the coil head.

[5] An arbitrary choice, but one that we believe to be appropriate. A different dimension could be chosen depending upon the coil application.

[6] Taking a mean over depth seems like a poor metric since $\widehat{S}_{\mathrm{gm}}$ decreases dramatically with depth. This would be true for an arithmetic mean because the strong responses would overwhelm the weak responses, but it is not true for the geometric mean because it equally weighs the strong and weak responses. The geometric mean can be thought of as an arithmetic mean of the log of the response.

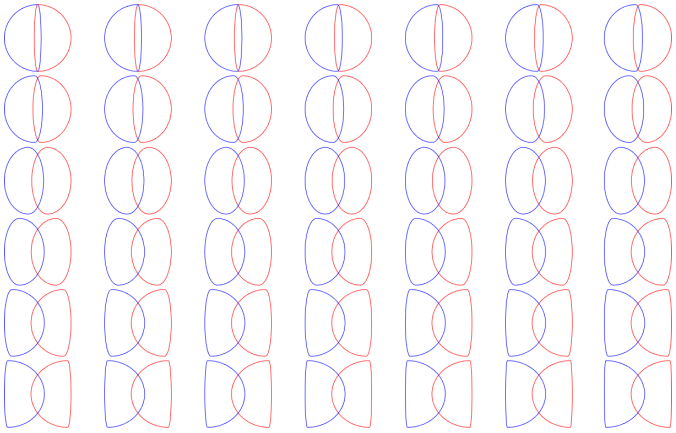

Fig. 3. Subset of the double-D coils being analyzed.

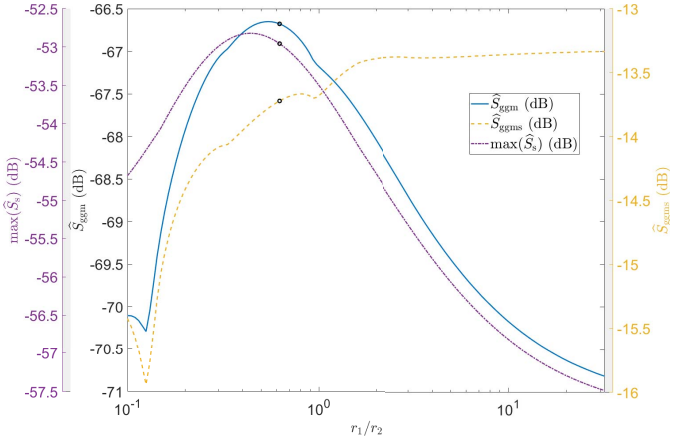

Fig. 4. $\widehat{S}_{\text{ggm}}$, $\widehat{S}_{\text{ggms}}$, and $\max\left(\widehat{S}_{\text{s}}\right)$ for the range of double-D coils. The optimal coil is marked on each curve with a black circle.

Metrics from the previous sections are calculated as the coil heads are permuted, and the best coils of each type can then be determined and compared to one another. All coils are constrained to fit into a square box with side lengths of $2r$ by $2r$.

These coil heads are generally constructed as tightly wound multi-turn coils. The windings are generally sufficiently close together so that they can be accurately modeled as a single large turn for the purpose of computing their magnetic fields. Then the normalized metrics, (8) and (14), will be essentially the same whether applied to the multi-turn coil or the single turn approximation because the length of the wire used in the metrics is proportional to the number of turns in the coil. For simplicity, the coils modeled here will use this single wire approximation. Note that the un-normalized metrics for the multi-turn and single turn approximation will also be essentially the same when the quantities such as the transmit power, the volumes of the conductors, receiver bandwith, etc. are the same.

A. Double-D Coils

An example of the double-D coil head geometry chosen for analysis is shown in Fig. 2. The coils are constrained to both fit in and fill a box that is $2r$ on each side. Each coil is made out of the halves of two ellipses with the same semi-major axis and different semi-minor axes, r_1 and r_2. During analysis, the ratio r_1/r_2 is swept over $10^{-1} < r_1/r_2 < 10^{1.5}$, while the overall width of each coil is determined by the overlap needed to null the coupling between the transmit and receive coils. A subset of the coils created for analysis is shown in Fig. 3.

The metrics $\widehat{S}_{\text{ggm}}$, $\widehat{S}_{\text{ggms}}$, and $\max\left(\widehat{S}_{\text{s}}\right)$ are calculated over the range of r_1/r_2 and plotted in Fig. 4 against r_1/r_2, and $\widehat{S}_{\text{ggm}}$ and $\widehat{S}_{\text{ggms}}$ are also plotted against one another as a black line in Fig. 25.

The optimal coil is much more apparent in Fig. 25 than in Fig. 4, illustrating the difficulty of choosing an optimal coil based on separate graphs of $\widehat{S}_{\text{ggm}}$, $\widehat{S}_{\text{ggms}}$, and $\widehat{S}_{\text{s}}$. Note how $\widehat{S}_{\text{ggm}}$ and $\widehat{S}_{\text{s}}$ are roughly correlated, but $\widehat{S}_{\text{ggm}}$ and $\widehat{S}_{\text{ggms}}$ are poorly correlated. The best coil head is chosen and plotted as a circle on Figs. 4 and 25. The geometry of the optimized coil head, for which $r_1/r_2 = 0.623$, is shown in Fig. 2. It has $\widehat{S}_{\text{ggm}} = -66.68$ dB and $\widehat{S}_{\text{ggms}} = -13.72$ dB.

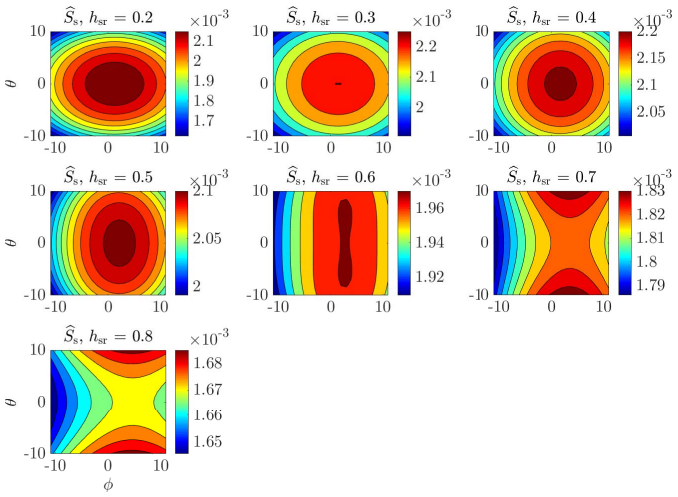

Fig. 5. Optimal double-D soil sensitivity for various heights above the soil and tilts relative to the soil.

Fig. 5 shows soil sensitivity cuts at various heights above the soil and tilts about the x-axis (θ) and the y-axis (ϕ) in degrees. The graphs appear off-center because the two coils of the double-D do not lie in exactly the same plane—there is an offset of $r/60$ in the z-direction to avoid nonphysical solutions resulting from overlapping coil turns. Interestingly, as the double-D is tilted, its soil sensitivity tends to improve. Figs. 6 and 7 illustrate the narrow cross-track and broad down-track sensitivity pattern of the double-D.

B. Concentric Coils

Now we will analyze concentric coil heads, such as the one pictured in Fig. 8a. This coil head consists of a single transmit coil and a receive coil with two counterwound sections, one inner and one outer. The mutual inductance between the transmit and receive coils is nulled by adjusting the turns ratio between the inner and outer sections of the receive coil. In the figure, the turns ratio, n, is two: $n = t_{\text{RX,inner}}/t_{\text{RX,outer}}$ (where t is

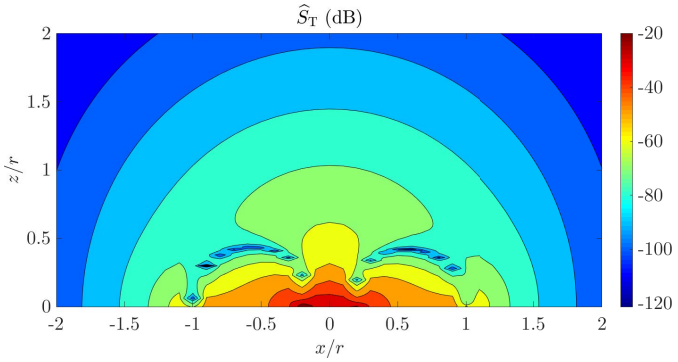

Fig. 6. Optimal double-D x-z plane target sensitivity cut.

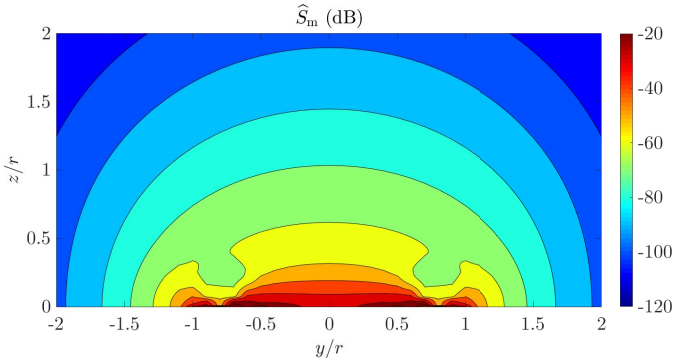

Fig. 7. $\widehat{S}_{\mathrm{m}}$ of the optimal double-D coil head.

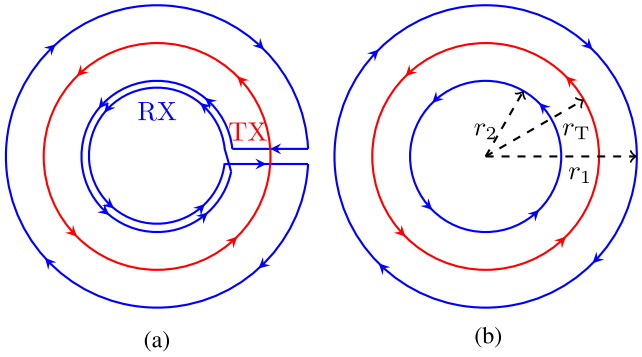

Fig. 8. Illustration of a normal concentric coil and the concentric coil model used for coil optimization. (a) Concentric coil head geometry. (b) Modified concentric coil head geometry.

the number of turns). It is assumed that the turns are tightly wound, so that the radius of each turn in a bundle is the same.

In order to simplify the representation, the coils are modeled differently from the coil head shown in Fig. 8a, ignoring the connection between the inner and outer portions of the receive coil. There are now effectively two receive coils, and the weighted sum of the voltage at the "terminals" of each receive coil will be the total received voltage (Fig. 8b).

The single transmit coil has radius r_{T} and the two counter-wound receive coils have radii r_1 and r_2, respectively. Each receive coil is modeled with a single turn, so the turns ratio is now analogous to a ratio of currents, $n = I_{\mathrm{RX1}}/I_{\mathrm{RX2}}$, where I_{RX1} and I_{RX2} are the currents flowing in the two receive coils. The transmit coil is spaced $r/25$ away from the receive coil in the z-direction to avoid nonphysical solutions where the two coils could become superimposed.

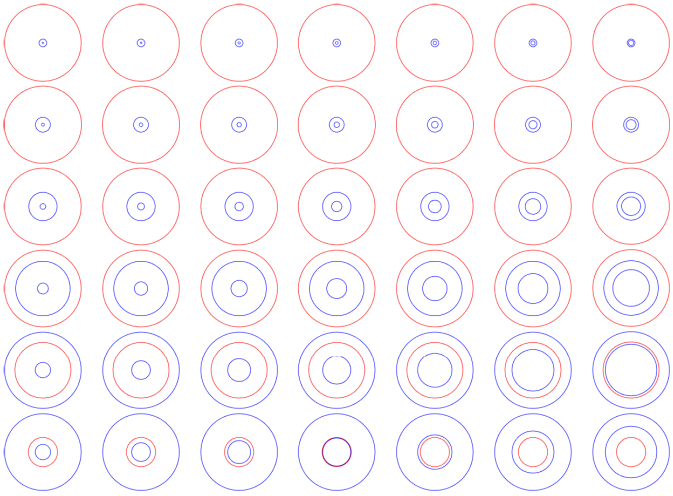

Fig. 9. Subset of the concentric coils being analyzed.

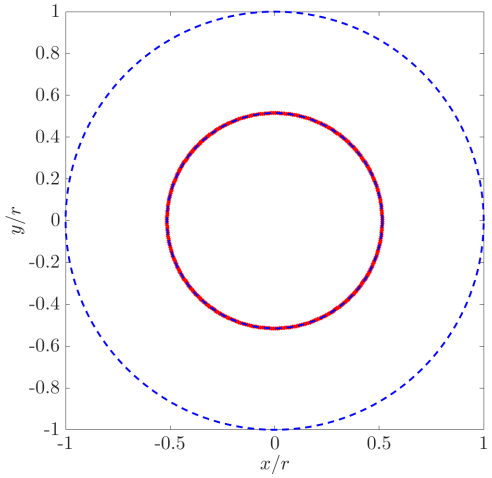

Fig. 10. Optimal concentric coil geometry.

The coils are parameterized by two ratios, $\alpha_{\mathrm{T}} = r_{\mathrm{T}}/r_1$ and $\alpha_{\mathrm{R}} = r_2/r_1$, and the two parameters are swept over the ranges $10^{-0.7} < \alpha_{\mathrm{T}} < 10^{1}$ and $10^{-0.7} < \alpha_{\mathrm{R}} < 10^{-0.1}$. With the geometry set for each α_{T} and α_{R}, the turns ratio that gives null coupling between the transmit and receive coils is calculated. This turns ratio is

$$n = \frac{M_{\mathrm{TX,RX1}}}{M_{\mathrm{TX,RX2}}}, \tag{19}$$

where $M_{\mathrm{TX,RX1}}$ is the mutual inductance between the transmit coil and the first receive coil, and $M_{\mathrm{TX,RX2}}$ is the mutual inductance between the transmit coil and the second receive coil [13]. A subset of the range of concentric coils being analyzed is shown in Fig. 9.

Once again, $\widehat{S}_{\mathrm{ggm}}$ and $\widehat{S}_{\mathrm{ggms}}$ are calculated for the range of coils and plotted in Fig. 25 as a red area. The optimal coil is then chosen and plotted on the same graph as a black x.

The optimized coil has $\widehat{S}_{\mathrm{ggm}} = -60.95$ dB and $\widehat{S}_{\mathrm{ggms}} = -17.85$ dB, and the geometry is shown in Fig. 10. The coil head has $\alpha_t = 0.51$ and $\alpha_r = 0.51$, and thus the transmit coil

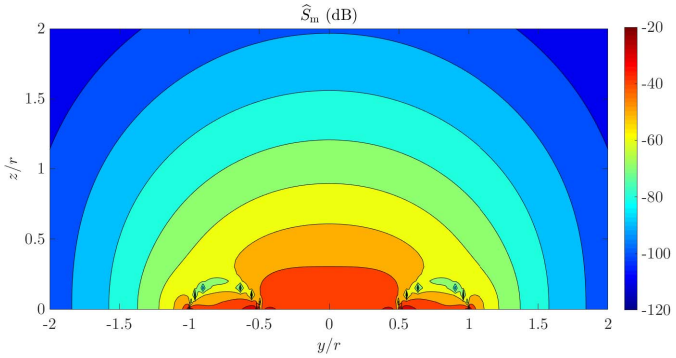

Fig. 11. $\widehat{S}_{\mathrm{m}}$ of the optimal concentric coil.

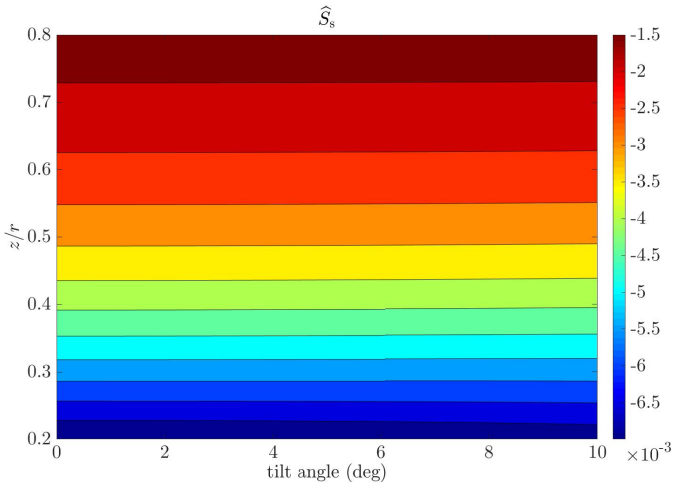

Fig. 12. Soil sensitivity of the optimal concentric coil for many heights above the soil and tilts relative to the soil.

and inner receive coil have the same radius. The turns ratio of the receive coil is 0.092. The broad target sensitivity pattern of this concentric coil head is illustrated in Fig. 11, and the soil sensitivity of this coil versus height above the soil and tilt relative to the soil is shown in Fig. 12. The symmetry of concentric coils causes an interesting property—as the coil head is tilted, the soil sensitivity remains largely constant.

Figs. 13 and 14 show the values of $\widehat{S}_{\mathrm{ggm}}$ and $max\left(\left|\widehat{S}_{\mathrm{s}}\right|\right)$ for each coil head that was considered. On these two graphs, $\widehat{S}_{\mathrm{ggm}}$ is roughly correlated with soil sensitivity, $\widehat{S}_{\mathrm{s}}$. The ratio of these two quantities is shown in Fig. 15. The correlation between Figs. 13 and 15 is less clear than that between $\widehat{S}_{\mathrm{ggm}}$ and $\widehat{S}_{\mathrm{s}}$—hence the need for a ratio. Comparing Fig. 15 to Fig. 13, we see how a coil that appears good when considering $\widehat{S}_{\mathrm{ggms}}$—for example, any of the coils in the top portion with $\widehat{S}_{\mathrm{ggms}} = -5$ dB—is $\sim$ 70 dB down in raw target sensitivity compared to the best coils in Fig. 13.

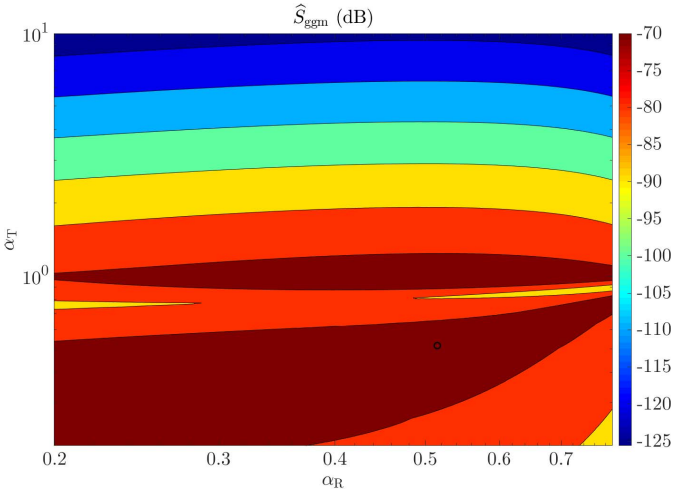

Fig. 13. $\widehat{S}_{\mathrm{ggm}}$ for many concentric coils. The optimal coil is marked with a circle.

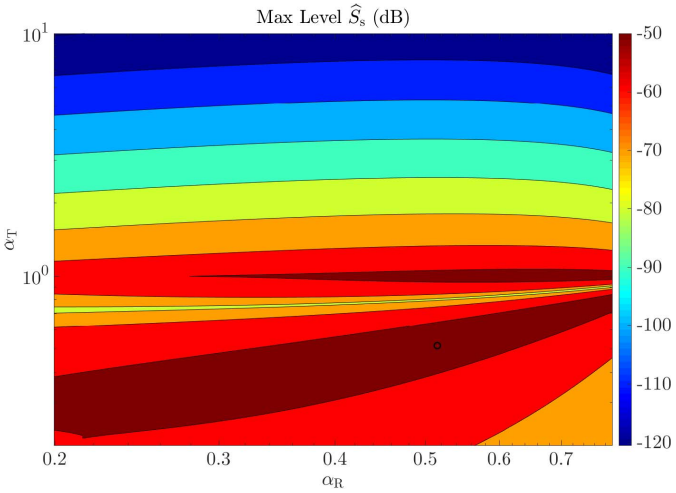

Fig. 14. Maximum of the soil sensitivity for each concentric coil head.

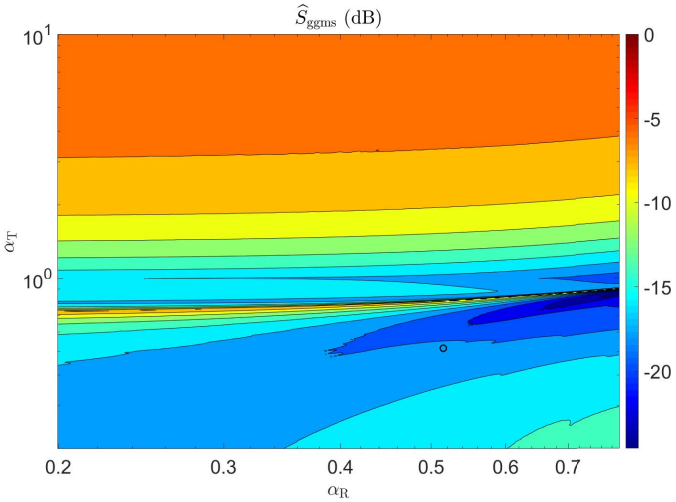

Fig. 15. $\widehat{S}_{\mathrm{ggms}}$ for many concentric coils. The optimal coil is marked with a circle.

C. Dipole/Quadrupole Coils

Finally, a dipole/quadrupole coil head is optimized. The dipole coil is the transmit, and the quadrupole coil (a figure-8) is the receive coil that provides the nulled coupling between the two coils. The geometry of the coil is shown in Fig. 16. Two parameters are varied during the optimization: c_{r}, the maximum radius of the dipole, and c_{s}, the spacing between the two coils. In calculating the shape of the dipole coil, the point at which c_{r} intersects the bounding box is where the coil is flattened against the box, and the corners are smoothly

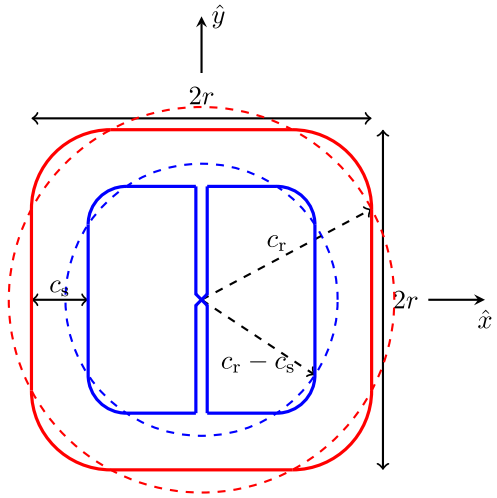

Fig. 16. Dipole/quadrupole coil geometry with dipole in red and quadrupole in blue.

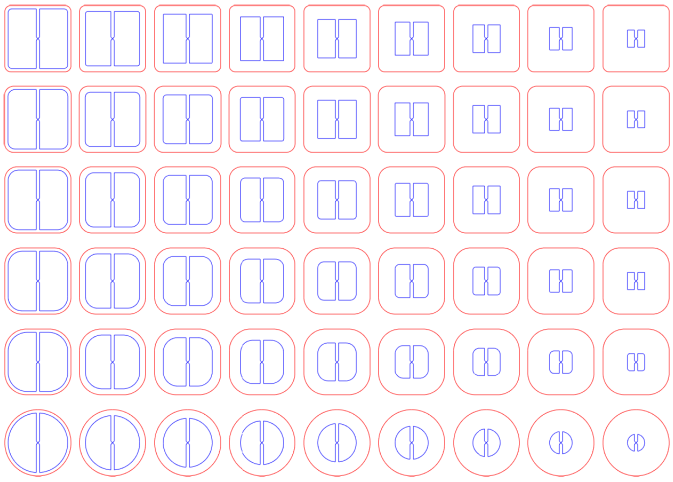

Fig. 17. Subset of the dipole/quadrupole coils being analyzed.

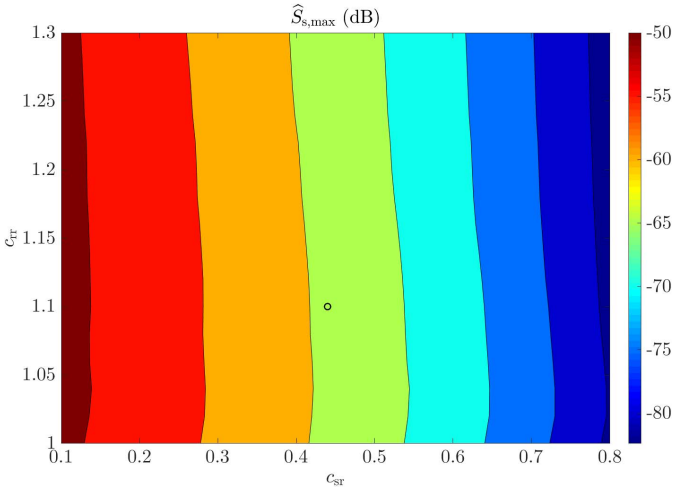

Fig. 18. Maximum dipole/quadrupole soil sensitivity for all coil heads considered.

radiused. A similar strategy is used for the quadrupole with a bounding box with sides equal to $2r - 2c_s$.

The variables c_r and c_s are taken to be in relation to the size of the bounding box as $c_{rr} = c_r/r$ and $c_{sr} = c_s/r$ and

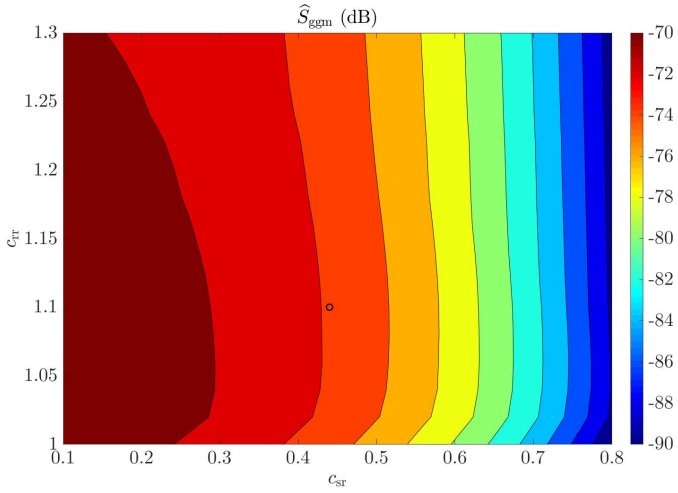

Fig. 19. $\widehat{S}_{ggm}$ in dB as a function of c_{rr} and c_{sr} for dipole/quadrupole coil heads.

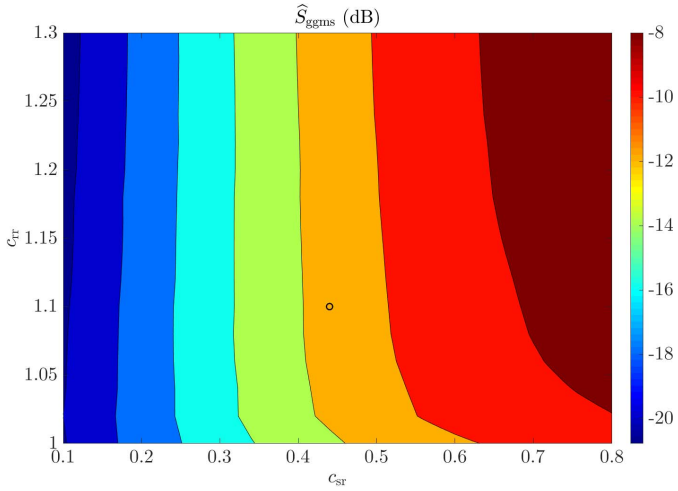

Fig. 20. $\widehat{S}_{ggms}$ as a function of c_{rr} and c_{sr} for all dipole/quadrupole coil heads.

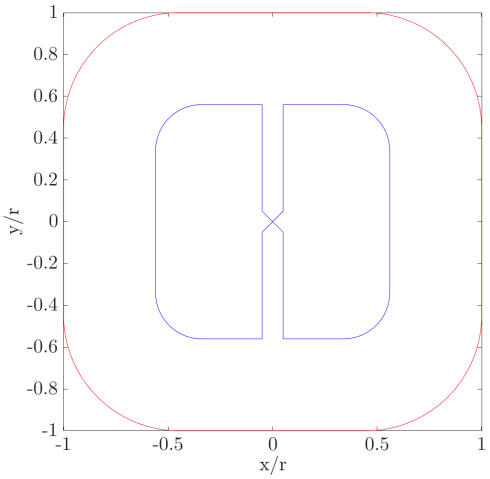

Fig. 21. Optimal dipole/quadrupole coil.

are swept over 1 <= c_{rr} <= 1.3 and 0.1 <= c_{sr} <= 0.8. A subset of the dipole/quadrupole coils being analyzed is shown in Fig. 17

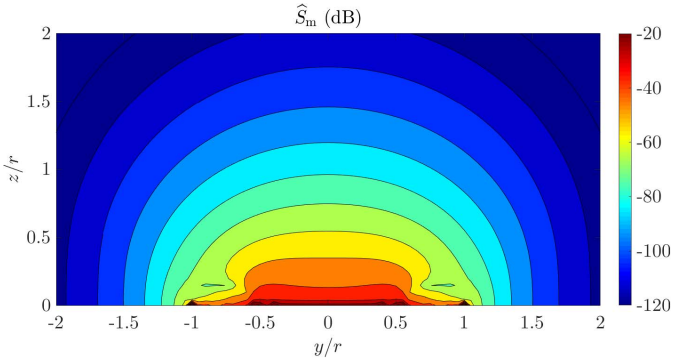

Fig. 22. $\widehat{S}_{\mathrm{m}}$ of the optimal dipole/quadrupole coil head.

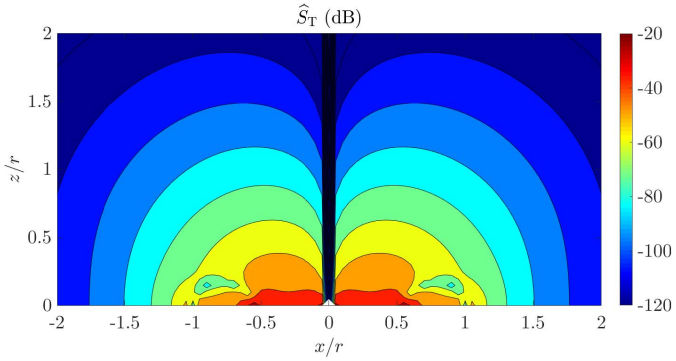

Fig. 23. Target sensitivity in the x-z plane of the optimal dipole/quadrupole coil head.

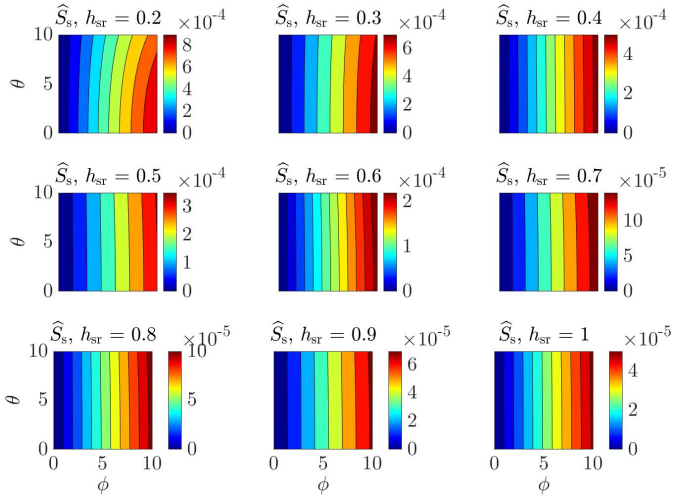

Fig. 24. The soil sensitivity of the optimal dipole/quadrupole coil over a range of heights above the soil and tilts relative to the soil.

Fig. 19 shows $\widehat{S}_{\mathrm{ggm}}$ for all the coil heads and Fig. 18 the maximum soil sensitivity with the optimal coil marked with a black circle. The target sensitivity is roughly correlated with the soil sensitivity, and roughly inversely correlated with $\widehat{S}_{\mathrm{ggms}}$. However, the correlation is once again not good enough to choose an optimal coil solely from $\widehat{S}_{\mathrm{ggm}}$ or $\widehat{S}_{\mathrm{s}}$.

The optimal coil head geometry, which has $c_{\mathrm{sr}} = 0.44$ and $c_{\mathrm{rr}} = 1.1$, is shown in Fig. 21. This coil head has $\widehat{S}_{\mathrm{ggm}} = -72.21$ dB and $\widehat{S}_{\mathrm{ggms}} = -11.3$ dB and is denoted on Fig. 25

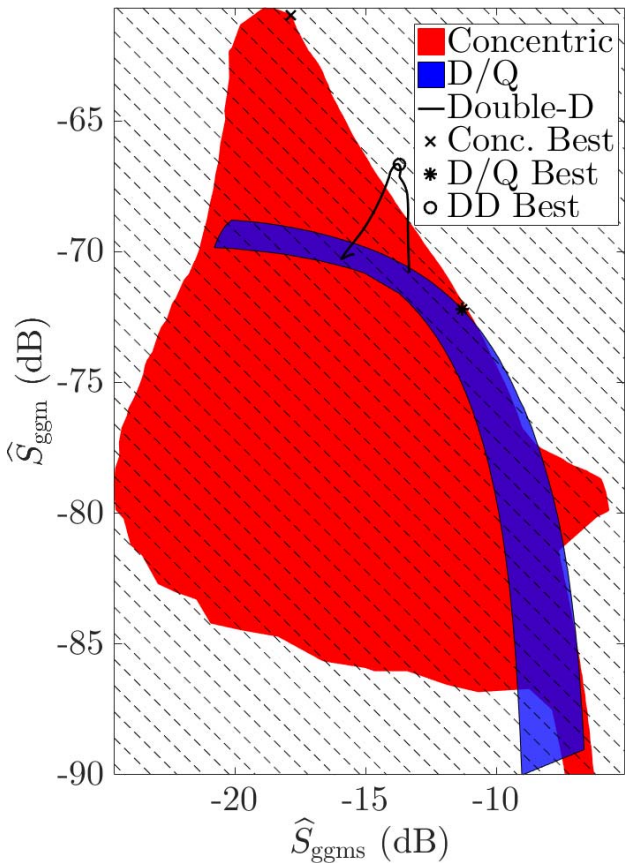

Fig. 25. Plot of the volume sensitivity against the ratio of the volume sensitivity to soil sensitivity for all the coils considered in this paper. The red and blue regions span all the coils swept during optimization for the concentric and dipole/quadrupole coil heads, respectively. The black line denotes the double-D coil heads, and the markers are the optimal coils from each set.

by a black star. The sensitivity graphs in Figs. 22 and 23 illustrate the off-center maximum sensitivity and nulled on-axis sensitivity of the dipole/quadrupole. Finally, Fig. 24 is a graph of the soil sensitivity for various soil heights and tilts. The dipole/quadrupole soil sensitivity shows very little variation when tilted down-track, but it changes quite a bit when tilted cross-track. Of course, there is very little soil sensitivity at all (in the ideal case, it would be zero) when the coil head is level. It should be noted that, since the dipole/quadrupole soil sensitivity worsens instead of improves when it is tilted, the apparent target sensitivity performance of the dipole/quadrupole head relative to the soil sensitivity can be altered by adjusting the maximum tilt about the y-axis.

VI. Conclusion

Now the optimized coil heads can be compared to one another and their traits summarized. Fig. 25 is a plot of the $\widehat{S}_{\mathrm{ggm}}$ against $\widehat{S}_{\mathrm{ggms}}$ for all the coils considered in this paper. The red and blue regions span all the coil head configurations considered during optimization for the concentric and dipole/quadrupole coil heads, respectively, and the black line is the double-D coil heads. Within the geometries that are reasonable to produce, the concentric coil heads give the most opportunity for tweaking performance, while the double-D

TABLE I
OPTIMAL COIL METRICS

Coil Performance		
Coil head	$\widehat{S}_{\text{ggm}}$ (dB)	$\widehat{S}_{\text{ggms}}$ (dB)
Concentric	-60.95	-17.85
Double-D	-66.68	-13.72
Dipole/quadrupole	-72.21	-11.3

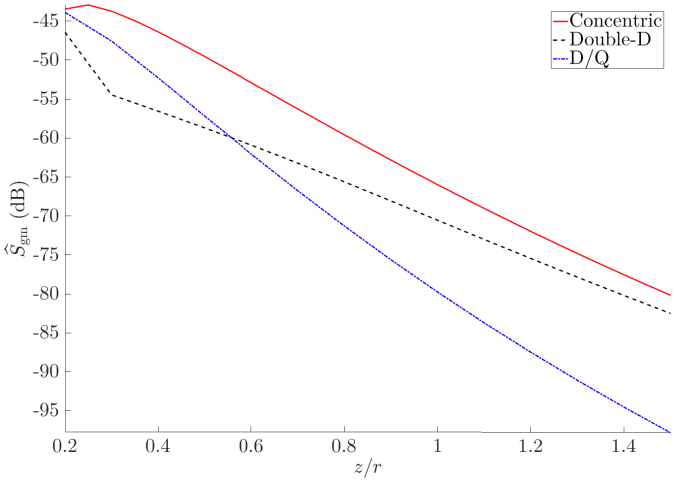

Fig. 26. $\widehat{S}_{\text{gm}}$ vs depth for each optimal coil.

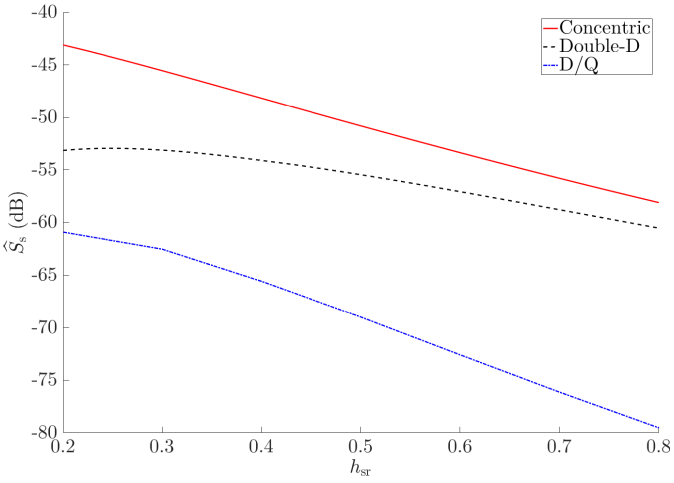

Fig. 27. $\widehat{S}_{\text{s}}$ vs height for all three optimal coils.

performance varies very little with shape. The region for the dipole/quadrupole is somewhat misleading because altering the amount of tilt changes the maximum soil response of the dipole/quadrupole. The dashed lines are lines of constant $\Delta\widehat{S}_{\text{ggm}}/\Delta\widehat{S}_{\text{ggms}}$, so moving along one of the dashed lines gives a constant tradeoff between target and soil sensitivity.

By this metric, the concentric coil head performs the best, the double-D is 2 dB down, and the dipole/quadrupole is 3 dB below the double-D. As can be seen in Fig. 8a or read from Table I, the order in terms of mean target sensitivity is the same, and performance of the various coils is reversed when the soil is considered. Fig. 26 is a plot of $\widehat{S}_{\text{gm}}$, and Fig. 27 shows the maximum soil sensitivity of the three coils versus soil height. By considering Figs. 25, 26, and 27 together, a good picture of the each coil head's performance can be formed.

The concentric coil head has very good target sensitivity at all depths but the worst soil rejection, so it would perform best in lightly mineralized soils. The double-D peforms less well than the concentric in terms of target sensitivity but much better when the soil is considered, hence its position as a good all-around coil that performs well in moderately mineralized soils. Finally, the dipole/quadrupole suffers with depth penetration as a result of the quadrupole receive coil, but its soil rejection is very good.

Common coil head types have been optimized and analyzed using metrics that remove various factors that influence coil head performance other than coil winding patterns. These results can be used for comparison to new coil head designs—such as those optimized using our partially convex algorithm—to determine their performance relative to existing coil heads [6].

REFERENCES

[1] G. Overton and C. Moreland, *Inside the Metal Detector*. Sweet Home, OR, USA: Geotech Press, 2012.
[2] Y. Das, "Effects of soil electromagnetic properties on metal detectors," *IEEE Trans. Geosci. Remote Sens.*, vol. 44, no. 6, pp. 1444–1453, Jun. 2006.
[3] P. Druyts, Y. Das, C. Craeye, and M. Acheroy, "Modeling the response of electromagnetic induction sensors to inhomogeneous magnetic soils with arbitrary relief," *IEEE Trans. Geosci. Remote Sens.*, vol. 47, no. 8, pp. 2627–2638, Aug. 2009.
[4] M. A. Reed and W. R. Scott, Jr., "Formulation of a method for the optimization of coils for electromagnetic induction systems in the presence of magnetic soil," in *Proc. IEEE Int. Geosci. Remote Sens. Symp. (IGARSS)*, Jul. 2015, pp. 4304–4307.
[5] M. A. Reed and W. R. Scott, Jr., "Improved method for the optimization of coils in the presence of magnetic soil," in *Proc. IEEE Int. Geosci. Remote Sens. Symp. (IGARSS)*, Jul. 2016, pp. 7489–7492.
[6] M. A. Reed and W. R. Scott, Jr., "Formulation for a practical implementation of electromagnetic induction coils optimized using stream functions," *Proc. SPIE*, vol. 9823, p. 982304, May 2016.
[7] C. E. Baum, "Two-dimensional coils for low-frequency magnetic illumination and detection," *Sensor Simul. Notes*, vol. 406, pp. 1–49, Nov. 1996.
[8] C. E. Baum, "Three-dimensional coils for low-frequency magnetic illumination and detection," *Sensor Simul. Notes*, vol. 411, pp. 1–64, May 1997.
[9] S. Kim and S. Yoo, "Comparison of planar type coils for efficient power supply to implantable devices," *Biomed. Eng. Lett.*, vol. 2, no. 3, pp. 179–185, Sep. 2012.
[10] R. Pellicer-Guridi, M. W. Vogel, D. C. Reutens, and V. Vegh, "Towards ultimate low frequency air-core magnetometer sensitivity," *Sci. Rep.*, vol. 7, no. 1, 2017, Art. no. 2269.
[11] X. Wu *et al.*, "Comparison of RF body coils for MRI at 3 T: A simulation study using parallel transmission on various anatomical targets," *NMR Biomed.*, vol. 28, pp. 1332–1344, Oct. 2015.
[12] P. Druyts, "Analysis of environmental effects on electromagnetic induction sensors," Ph.D. dissertation, Inst. Inf. Commun. Technol., Electron. Appl. Math., Universite Catholique de Louvain, Louvain-la-Neuve, Belgium, Oct. 2011. [Online]. Available: http://hdl.handle.net/2078.1/94326
[13] M. A. Reed and W. R. Scott, Jr., "Metrics for the comparison of coils used in electromagnetic induction systems," *Proc. SPIE*, vol. 10182, p. 1018213, May 2017.
[14] M. A. Reed and W. R. Scott, Jr., "Analysis of double-D induction coil performance in magnetic soils using new coil metrics," in *Proc. Int. Geosci. Remote Sens. Symp. (IGARSS)*, Jul. 2017, pp. 3732–3735.
[15] H. Vesselle and R. E. Collin, "The signal-to-noise ratio of nuclear magnetic resonance surface coils and application to a lossy dielectric cylinder model—Part I: Theory," *IEEE Trans. Biomed. Eng.*, vol. 42, no. 5, pp. 497–506, Aug. 1995.

[16] W. C. Chew, *Waves and Fields in Inhomogeneous Media*. Piscataway, NJ, USA: IEEE Press, 1995, pp. 485–487.
[17] F. E. Neumann, "Allgemeine Gesetze der inducirten elektrischen Ströme," *Annalen der Physik*, vol. 146, no. 1, pp. 31–44, 1846.
[18] W. R. Smythe, *Static and Dynamic Electricity*. New York, NY, USA: McGraw-Hill, 1950, pp. 310–316.

Mark A. Reed received the B.S.E.E. and M.S.E.C.E. degrees from the Georgia Institute of Technology in 2009 and 2011, respectively, where he is currently pursuing the Ph.D. degree with the School of Electrical and Computer Engineering. His interests include applied electromagnetics with applications to the detection of subsurface objects.

Waymond R. Scott, Jr. (F'08) is currently the Joseph M. Pettit Professor with the School of Electrical and Computer Engineering, Georgia Institute of Technology. His research involves the interaction of electromagnetic and elastic fields with materials. This research spans a broad range of topics, including the measurement of the properties of materials, experimental and numerical modeling, and systems for the detection of buried objects. He has published over 60 refereed journal papers and 160 conference papers. He has received over $12 M of research funding over the last 15 years from three multi-university research initiatives as well as single investigator projects from ONR, ARO, the U.S. Army, and the U.S. Army Corps of Engineers. He received the 1986 Andrew Chi Prize Paper Award for the best paper published in the IEEE TRANSACTIONS ON INSTRUMENTATION AND MEASUREMENT, the 2002 Symposium Prize Paper Award for the best paper presented at the IEEE 2001 International Geoscience and Remote Sensing Symposium, and the 2013 EURASIP Best Paper Award for the best paper published in the *Signal Processing Journal*. His students received four other best paper awards.